

The effect of dynamical Bloch oscillations on optical-field-induced current in a wide gap dielectric

Péter Földi,^{1,*} Mihály G. Benedict,¹ and Vladislav S. Yakovlev^{2,3,†}

¹*Department of Theoretical Physics, University of Szeged,
Tisza Lajos körút 84-86, H-6720 Szeged, Hungary*

²*Ludwig-Maximilians-Universität, Am Coulombwall 1, 85748 Garching, Germany*

³*Max-Planck-Institut für Quantenoptik, Hans-Kopfermann-Straße 1, 85748 Garching, Germany*

We consider the motion of charge carriers in a bulk wide gap dielectric interacting with a few-cycle laser pulse. A semiclassical model based on Bloch equations is applied to describe the emerging time dependent macroscopic currents for laser intensities approaching the damage threshold. At such laser intensities, electrons can reach edges of the first Brillouin zone even for electron-phonon scattering rates as high as those known for SiO₂. We find that, whenever this happens, Bragg-like reflections of electron waves, also known as Bloch oscillations, affect the dependence of the charge displaced by the laser pulse on its carrier-envelope phase.

I. INTRODUCTION

The motion of conduction electrons in a crystalline solid is usually considered to be similar to that in free space, apart from scattering processes. The situation is radically different in the case where an external electric field is so strong that, in spite of scattering, an electron can acquire such a high quasimomentum that it reaches an edge of the first Brillouin zone. While the kinetic energy of a free electron exposed to a constant external field would indefinitely increase, an electron in a crystal first slows down until it reaches the top of the energy band, and then it moves in the opposite direction towards the bottom of the band. In the semiclassical picture neglecting scattering, the electron would move periodically back and forth between its initial and final positions. This phenomenon is known as Bloch oscillations [1], and it leads to Wannier–Stark localization [2]. In the reciprocal space, an electron reaching an edge of the first Brillouin zone continues its motion from the opposite side of the zone. In the real space, this corresponds to a Bragg-like reflection of an electron wave [3]. While Bloch oscillations and Wannier–Stark localization are usually considered in the case of a constant external field, essentially the same physical phenomena take place if the external field is time dependent. In this paper, we use the term ‘dynamical Bloch oscillations’ (DBOs) to describe phenomena that occur whenever an electron wave is reflected at an edge of the Brillouin zone.

Until recently, Bloch oscillations were thought to be impossible to observe in bulk solids because of scattering. The period of Bloch oscillations in a constant field F is given by $T_B = \hbar/(eFa)$, where \hbar is the Planck constant and a is a lattice period. To observe Bloch oscillations, T_B must be smaller than characteristic scattering and dephasing times, which are usually on the order of

$T_s \sim 10^{-13}$ s. This implies that the external field must be stronger than $F \gtrsim \hbar/(eaT_s) \sim 10^8$ V m⁻¹. Such a strong constant field would destroy even wide gap dielectrics. Therefore, over the last few decades, Bloch oscillations were predominantly studied in semiconductor superlattices [4–10] and optical lattices [11].

The situation has recently changed as intense few-cycle pulses were generated in the mid-infrared (MIR) spectral region [12], and the duration of the shortest near-infrared (NIR) pulses approached one optical cycle [13]. Ghimire *et al.* [14, 15] observed that anharmonicity in the motion of charge carriers created and driven by an intense MIR pulse in ZnO resulted in the generation of high-order harmonics [16] and a red-shift of absorption edge. In their parameter regime, the field was intense enough to drive conduction electrons beyond the first Brillouin zone, so that Bloch oscillations were suggested to be responsible for the observed effects. Very recently, Schiffrin *et al.* [17] have found that a 4 fs NIR pulse with a peak electric field of 20 GV m⁻¹ can induce measurable currents in a SiO₂ sample. Furthermore, it has been found that these currents can be steered by controlling the carrier-envelope phase (CEP) [18] of laser pulses. These findings were interpreted in terms of Wannier–Stark states [19].

While it remains debatable whether Bloch oscillations played a major role in these particular measurements, there is no doubt that intense few-cycle pulses enable experiments in the parameter regime where electrons in a bulk solid are accelerated beyond the first Brillouin zone. The purpose of this paper is to study some basic effects related to this parameter regime. In particular, we consider the role of electron scattering and dephasing.

Electron–phonon scattering rates are known to be particularly high for SiO₂ due to a strong coupling between conduction electrons and longitudinal optical (LO) phonons [20, 21]. At the same time, scattering rates for moderately hot ($E_{\text{kin}} \sim 1$ eV) electrons, which we consider in this paper, have never been measured directly, and there are still open questions related to the scattering of very hot conduction electrons [22].

*Electronic address: foldi@physx.u-szeged.hu

†Electronic address: vladislav.yakovlev@lmu.de

II. SYSTEM AND MODEL

We consider the following model (see Fig. 1): the xy ($z = 0$) plane is the surface of a dielectric. Short pulses with a stabilized CEP propagate along the z -axis and impinge on this surface. In our calculations, we assume that the external electric field within the sample is linearly polarized and given by $\mathcal{E}_x(t) = \mathcal{E}_0 \cos(\omega_0 t + \varphi_{\text{CEP}}) \exp(-\frac{t^2}{2\tau^2})$, $\mathcal{E}_y = \mathcal{E}_z = 0$.

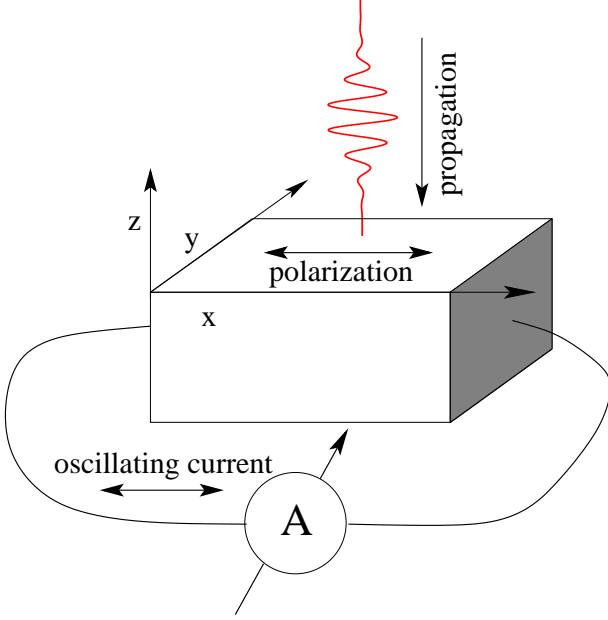


Figure 1: A schematic view of the creation and driving of macroscopic currents with a laser pulse. Measurements [17] yield the charge transferred by the pulse.

We adopt the two-band approximation and consider the electron motion in two spatial dimensions. At each moment t , we describe electronic excitations in the sample with the aid of quantum-mechanical density matrices

$$\rho(\mathbf{k}, t) = \begin{pmatrix} n_c(\mathbf{k}, t) & P(\mathbf{k}, t) \\ P^*(\mathbf{k}, t) & n_v(\mathbf{k}, t) \end{pmatrix}, \quad (1)$$

where n_c , n_v correspond to the conduction and valence band populations, the off-diagonal element $P(\mathbf{k}, t)$ represents the interband coherence, and the quasimomentum \mathbf{k} has two components: $\mathbf{k} = (k_x, k_y)$. The time dependence of the density matrix is formally described by

$$\frac{\partial}{\partial t} \rho(\mathbf{k}, t) = \left(\frac{\partial \rho}{\partial t} \right)_{\text{exc}} + \left(\frac{\partial \rho}{\partial t} \right)_{\text{field}} + \left(\frac{\partial \rho}{\partial t} \right)_{\text{scatt}}. \quad (2)$$

The three terms on the right-hand side of this equation

describe photoexcitation, the acceleration of charge carriers by the external field and electron scattering.

We chose to describe photoexcitation dipole transitions using the following form of \mathbf{k} resolved optical Bloch equations [23, 24]:

$$\begin{aligned} \frac{\partial P(\mathbf{k})}{\partial t} &= -\frac{i}{\hbar} [E_c(\mathbf{k}) - E_v(\mathbf{k}) - i\hbar\kappa] P(\mathbf{k}) \\ &\quad - i[n_c(\mathbf{k}) - n_v(\mathbf{k})] d_{cv}(\mathbf{k}) \mathcal{E}(t), \\ \frac{\partial n_c(\mathbf{k})}{\partial t} &= -2\Im[d_{cv}(\mathbf{k}) \mathcal{E}(t) P^*(\mathbf{k})], \\ \frac{\partial n_v(\mathbf{k})}{\partial t} &= -\frac{\partial n_c(\mathbf{k})}{\partial t}, \end{aligned} \quad (3)$$

where $E_v(\mathbf{k})$ and $E_c(\mathbf{k})$ are the energies of the valence and conduction bands, respectively.

The phenomenological rate κ describes the decay of the interband coherences. For simplicity, we estimate the dependence of the dipole matrix elements on \mathbf{k} as [24]

$$d_{cv}(\mathbf{k}) = d_{cv}(0) \frac{E_c(0) - E_v(0)}{E_c(\mathbf{k}) - E_v(\mathbf{k})}.$$

The actual value of $d_{cv}(0)$ has little qualitative effect on our results, as long as saturation-related phenomena are negligible, i.e. the excited population is well below unity. In the following, we use $d_{cv}(0) = 0.1$ atomic units. Note that Eqs. (3) make no use of the rotating wave approximation. This allows us to investigate dynamics that unfold within a single optical oscillation of the laser pulse. (See e.g. [25] for a detailed discussion of related phenomena.)

The external electric field not only causes transitions between the bands, but it also accelerates and decelerates charge carriers. These field-driven dynamics are accounted for by the second term in Eq. (2). We neglect off-diagonal terms in $\left(\frac{\partial \rho}{\partial t} \right)_{\text{field}}$ and evaluate the diagonal ones as

$$\left(\frac{\partial n_{v,c}(\mathbf{k})}{\partial t} \right)_{\text{field}} = -\frac{e}{\hbar} \mathcal{E}(t) \nabla_{\mathbf{k}} n_{v,c}(\mathbf{k}). \quad (4)$$

Note that $\mathcal{E}(t)$ includes the screening field due to the collective electron response [26] (i.e. it denotes the field that actually interacts with individual electrons).

The third term in Eq. (2) accounts for the loss of intraband coherence due to scattering, where longitudinal optical (LO) phonons are considered to play the major role. The electron-phonon interaction is described by the Fröhlich Hamiltonian, and standard methods [24] lead to the following dynamical equations:

$$\left(\frac{\partial n_c(\mathbf{k})}{\partial t}\right)_{\text{scatt}} = \gamma_0 \sum_{\mathbf{q}} \delta(E(\mathbf{k} + \mathbf{q}) - E_c(\mathbf{k}) - \hbar\omega_{\text{LO}}) \frac{1}{q^2} \left\{ -N_{\mathbf{q}} n_c(\mathbf{k}) [1 - n_c(\mathbf{k} + \mathbf{q})] + (N_{\mathbf{q}} + 1) n_c(\mathbf{k} + \mathbf{q}) [1 - n_c(\mathbf{k})] \right\} + \gamma_0 \sum_{\mathbf{q}} \delta(E(\mathbf{k} - \mathbf{q}) - E_c(\mathbf{k}) + \hbar\omega_{\text{LO}}) \frac{1}{q^2} \left\{ -(N_{\mathbf{q}} + 1) n_c(\mathbf{k}) [1 - n_c(\mathbf{k} - \mathbf{q})] + N_{\mathbf{q}} n_c(\mathbf{k} - \mathbf{q}) [1 - n_c(\mathbf{k})] \right\}, \quad (5)$$

where $\hbar\omega_{\text{LO}}$ denotes the energy of an LO phonon, which is assumed to be independent of the reciprocal-space vector \mathbf{q} . The related phonon density is denoted by $N_{\mathbf{q}}$, and γ_0 is an electron-phonon coupling constant. For the sake of simplicity, we use a tight-binding type dispersion relation, i.e. $E_c(\mathbf{k})$ is proportional to $2 - \cos(k_x a) - \cos(k_y a)$, where a is a lattice constant. At room temperature, the average thermal phonon number and, consequently, $N_{\mathbf{q}}$ are practically zero, so phonon emission processes (accompanied by electron scattering events with a loss of electron energy) dominate the scattering dynamics.

The model above allows us to calculate the rate of scattering on LO phonons $\gamma(\mathbf{k})$, which is proportional to γ_0 appearing in Eq. (5). This scattering rate determines how fast the quasimomentum of an electron wave packet decreases as a consequence of scattering events. Our numerical calculations show – in accordance with the analytical results presented e.g. in [21] – that the rate $\gamma(\mathbf{k})$ has a pronounced minimum at $|\mathbf{k}| = 0$, being nearly constant ($\gamma(\mathbf{k}) \approx \gamma$) for kinetic energies in the range between 0.5 eV and 2 eV. In the following, we use γ as a label to quantify the strength of electron-phonon interaction in different simulations, although we used \mathbf{k} dependent scattering rates in our calculations.

For our simulations, we used material parameters that correspond SiO₂: a band gap of 9 eV, lattice period $a = 0.5$ nm, two LO phonon modes with energies $\hbar\omega_{\text{LO}} = 0.153$ and 0.063 eV, and a combined scattering rate equal to $\gamma = 0.3$ fs⁻¹. The laser pulse parameters correspond to the experiment described in [17]: $\omega_0 = 2.51$ fs⁻¹ and $\tau = 2.3$ fs.

III. RESULTS

A. Electron acceleration in the laser field

Before we present simulations where a laser pulse creates and drives charge carriers, let us consider the laser-driven motion of an initially free electron neglecting interband transitions. Similar simulations can be found in [27]. As an example, we take the initial distribution of conduction electrons as a Gaussian wave packet centred at $\mathbf{k} = 0$, neglect the terms $\left(\frac{\partial \rho}{\partial t}\right)_{\text{exc}}$ and $\left(\frac{\partial \rho}{\partial t}\right)_{\text{scatt}}$ in Eq. (2) and model the time evolution of the electron wave packet by solving Eq. (4). We plot the distribution of conduction electrons in false-colour diagrams, where

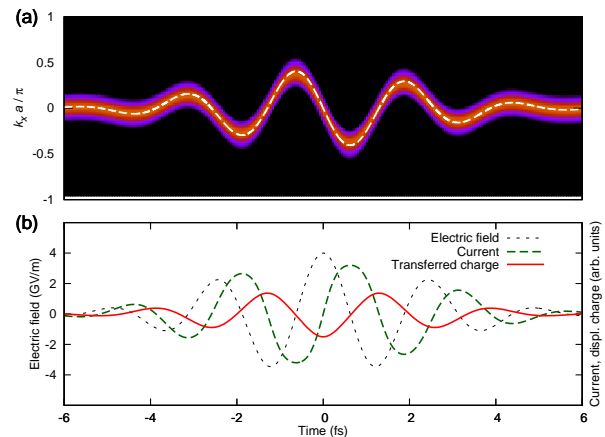


Figure 2: Time evolution of a wave packet initially centred at $\mathbf{k} = 0$ in a simulation that neglects photoexcitation and electron-phonon scattering. (a) The distribution of conduction electrons $n_c(\mathbf{k}, t)$ in the $k_y = 0$ plane. The dashed white line is the 'semiclassical trajectory' evaluated with the aid of the acceleration theorem (6). (b) The electric field $\mathcal{E}_x(t)$ that drives the wave packet, the current density $j_x(t)$ and the time dependent transferred charge $Q(t)$. The parameters are $\mathcal{E}_0 = 4$ GV m⁻¹, $\varphi_{\text{CEP}} = 0$, $\tau = 2.3$ fs.

colours vary from black through red to yellow as the electron density $n_c(\mathbf{k}, t)$ grows from zero to its maximal value. The top panel of Fig. 2 presents such a diagram in the plane $k_y = 0$. In this example, the distribution remains localized in the reciprocal space, and it is dynamically shifted by the field of the laser pulse. The reciprocal-space motion of the wave packet is appropriately described by the 'acceleration theorem' [28]:

$$\frac{\partial \mathbf{k}}{\partial t} = -\frac{e}{\hbar} \mathcal{E}(t). \quad (6)$$

A solution of this equation with the initial condition $\mathbf{k}(t_{\text{min}}) = 0$ is shown by the dashed white line in Fig. 2. This solution can be regarded as a trajectory of a 'classical particle' in the reciprocal space. Let us note that as long as neither scattering nor excitation is taken into account, there is a simple scaling in the model: increasing both the carrier frequency ω_0 and the amplitude of the laser pulse \mathcal{E}_0 by a certain factor is equivalent to choosing a new unit of time in Eq. (2), and it does not change the maximal quasimomentum that a wave packet can reach

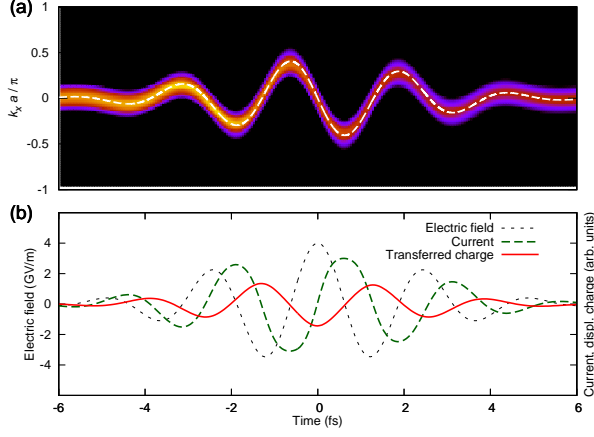


Figure 3: Time evolution of a wave packet initially centred at $\mathbf{k} = 0$ in a simulation that neglects photoexcitation but takes electron-phonon scattering into account. $\gamma = 0.3 \text{ fs}^{-1}$, all other parameters are the same as in Fig. 2.

in the reciprocal space.

Having evaluated the time evolution of the density matrix, we are to investigate measurable physical quantities. The time dependent current density $\mathbf{j}(t)$ is a sum of contributions from conduction-band electrons

$$\mathbf{j}_c(t) = \int_{\text{BZ}} e \mathbf{v}_c(\mathbf{k}) n_c(\mathbf{k}, t) d^2 \mathbf{k}, \quad (7)$$

valence-band holes

$$\mathbf{j}_v(t) = \int_{\text{BZ}} e \mathbf{v}_v(\mathbf{k}) n_v(\mathbf{k}, t) d^2 \mathbf{k}, \quad (8)$$

and interband coherences

$$\mathbf{j}_{cv}(t) = \frac{2}{\hbar} \Im \int_{\text{BZ}} P(\mathbf{k}, t) d_{cv}(\mathbf{k}) [E_v(\mathbf{k}) - E_c(\mathbf{k})] d^2 \mathbf{k}, \quad (9)$$

where the integrals are taken over the first Brillouin zone, and the velocity distributions are given by $\mathbf{v}_{v,c}(\mathbf{k}) = \frac{1}{\hbar} \nabla_{\mathbf{k}} E_{v,c}(\mathbf{k})$. Eqs. (7)-(9) result from evaluating the expectation value of the current operator averaged over a unit cell for a state described by the density matrix (1). Integrating the current density with respect to time, we obtain the charge that flows per a unit-area surface perpendicular to the x -axis: $Q(t) = \int_{-\infty}^t j_x(t') dt' = Q_c(t) + Q_v(t) + Q_{cv}(t)$, where j_x denotes the x component of the total current density $\mathbf{j} = \mathbf{j}_c + \mathbf{j}_v + \mathbf{j}_{cv}$. It is the charge displaced by the laser pulse $Q = Q(\infty)$ that can be measured in experiments [17]. In the following, we assume that \mathbf{j}_c gives the dominant contribution to Q . Indeed, \mathbf{j}_v is negligible in comparison with \mathbf{j}_c due to the low mobility of holes in the valence band, while \mathbf{j}_{cv} mainly describes the polarization response of valence-band electrons; according to our calculations, $Q_{cv}(t)$ is proportional to the applied field within a relative error of no more than 5%

up to a field amplitude of $\mathcal{E}_0 = 25 \text{ GV m}^{-1}$, $Q_{cv}(\infty)$ being negligibly small in comparison to $Q_c(\infty)$. With this in mind, we restrict our analysis to \mathbf{j}_c and Q_c , referring to them as 'current density' and 'transferred charge', respectively. These quantities are shown in Fig. 2(b), together with the electric field of the laser pulse, which is depicted by the dashed black line.

In Fig. 3, we show the effects of electron-phonon scattering on the dynamics of a conduction-band wave packet initially centred at $\mathbf{k} = 0$. A comparison with Fig. 2, where scattering was neglected, reveals that the electron-phonon interaction slightly reduces $j_x(t)$. This is explained by the fact that electrons get scattered out of the plane $k_y = 0$.

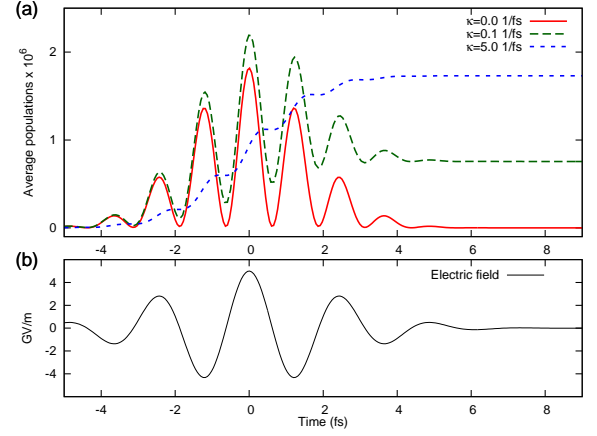


Figure 4: Average conduction-band population $\langle n_c \rangle = (\int d^2 \mathbf{k})^{-1} \int n_c(\mathbf{k}) d^2 \mathbf{k}$ for different interband coherence relaxation rates κ . For $\kappa = 5.0 \text{ fs}^{-1}$ (dashed blue curve), we plot $0.05 \langle n_c \rangle$. The parameters are $\mathcal{E}_0 = 5 \text{ GV m}^{-1}$, $\varphi_{\text{CEP}} = 0$, $\tau = 2.3 \text{ fs}$, $\gamma = 0.3 \text{ fs}^{-1}$.

B. Nonresonant interband excitations

In order to expose a medium to a very intense laser field without destroying it, the medium must be possibly transparent, so that little energy will remain in the medium after the interaction with the pulse. This implies that the laser frequency ω_0 should be much smaller than the bandgap. This is why we are interested in studying nonresonant excitations. With our laser parameters, it takes more than five laser photons to bridge the bandgap of SiO_2 .

The dynamics of interband excitations predicted by our model are shown in Fig. 4. For $\kappa = 0$, Eq. (3) describes a completely coherent excitation process, with the average population in the conduction band being roughly proportional to the laser intensity. These periodic excitations and deexcitations are sometimes referred to as 'virtual excitations', as they largely represent distortions

of initial electronic states. Both virtual and real excitations contribute to photocurrents [29]. In the opposite extreme, if we assume an unrealistically fast decoherence $\kappa = 5 \text{ fs}^{-1}$, the conduction band population becomes a monotonically increasing step-like function of time. Little is known about ultrafast dephasing in SiO_2 , so we use $\kappa = 0.1 \text{ fs}^{-1}$ for our further simulations as a value that corresponds to an intermediate regime of interband excitations.

C. Laser-driven motion of photoexcited charge carriers and the effect of the carrier-envelope phase

Here, we investigate outcomes of our model with all three terms of Eq. (2) being taken into account. The most interesting outcome of combining excitation and laser-driven motion is that this may result in a nonzero charge Q transferred by a laser pulse—a transport effect that does not occur in simulations neglecting interband transitions, as Figs. 2 and 3 illustrate. In this section, we show that this is a combination of interband transitions and a dispersion law that determines the transferred charge.

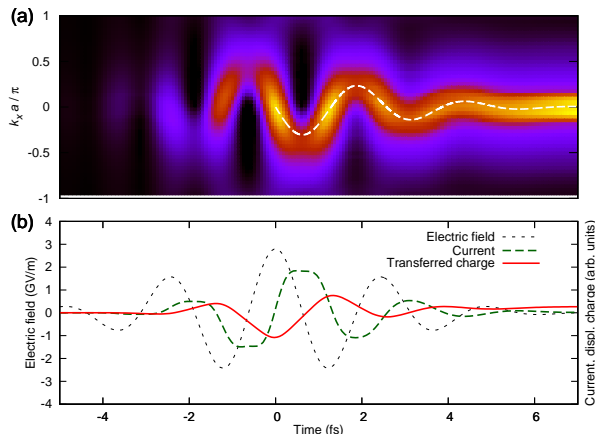


Figure 5: (a) Time evolution of the conduction-band electron population that emerges due to multiphoton excitations. The cross section in the k_x direction (parallel to the external field polarization) is shown for the following parameters: $\mathcal{E}_0 = 3 \text{ GV m}^{-1}$, $\varphi_{\text{CEP}} = 0$, $\tau = 2.3 \text{ fs}$, $\kappa = 0.1 \text{ fs}^{-1}$, $\gamma = 0.3 \text{ fs}^{-1}$. The dashed white line represent a semiclassical trajectory released at $t = 0$ with $\mathbf{k} = 0$. (b) The electric field of the laser pulse $\mathcal{E}_x(t)$, the induced current density $j_x(t)$ and the transferred charge $Q(t)$ as functions of time.

In the upper panels of Figs. 5 and 6, we show $n_c(k_x, t)$ obtained in simulations that account for all the relevant processes: multiphoton excitations, light-driven motion of charge carriers, dephasing and electron-phonon scattering. The simulation was performed for a ‘cosine’ ($\varphi_{\text{CEP}} = 0$) and a ‘sine’ ($\varphi_{\text{CEP}} = \pi/2$) laser pulses, respectively. The lower panels of the figures show the

electric field of the laser pulse $\mathcal{E}_x(t)$, the induced current density $j_x(t)$ and the transferred charge $Q(t)$ as functions of time. Because of scattering, the current density at the end of each simulation quickly approaches zero, but the final value of the transferred charge is in general nonzero, and it has a significantly higher value for the cosine pulse (Fig. 5).

The dashed lines in Figs. 5(a) and 6(a) represent ‘semi-classical electron trajectories’ released at a peak of the electric field, which are solutions of Eq. (6) with the initial condition $\mathbf{k}(t_0) = 0$, the initial time being $t_0 = 0$ for the cosine pulse and $t_0 = -\pi(2\omega_0)^{-1}$ for the sine pulse. Even without taking scattering into account, this semiclassical analysis can be used to explain many features observed in our calculations. In this picture, the contribution from a particular electron to the transferred charge at a final time t_{max} is determined by the semiclassical electron displacement:

$$\mathbf{s}(t_0) = \int_{t_0}^{t_{\text{max}}} \mathbf{v}_c(\mathbf{k}(t)) dt, \quad (10)$$

where t_0 is a time when the electron appeared in the conduction band, $\mathbf{k}(t)$ satisfies Eq. (6), $\mathbf{v}_c(\mathbf{k}) = \frac{1}{\hbar} \nabla_{\mathbf{k}} E_c(\mathbf{k})$ and an implicit assumption was made that the initial velocity of the electron is zero. In the case of a short cosine pulse, the central half-cycle of the electric field has a significantly higher amplitude than any other half-cycle. Consequently, there is one dominant semiclassical trajectory that starts at the peak of the main half-cycle. A simple calculation shows that, in our example, the semiclassical displacement associated with this trajectory is negative, which agrees with the positive final transferred charge in Fig. 5. For a short sine pulse, there are two dominant trajectories which start at the peaks of the two most pronounced half-cycles of the electric field. The electron displacements associated with these trajectories have opposite signs and ‘add destructively’ in the case shown in Fig. 6. This explains why the magnitude of the net transferred charge is considerably smaller for $\varphi_{\text{CEP}} = \pi/2$ than for $\varphi_{\text{CEP}} = 0$.

We further elaborate on the role of the CEP in Fig. 7, where we plot $Q(\varphi_{\text{CEP}})$ for different values of κ and γ . From this figure, one can see that $Q(\varphi_{\text{CEP}} + \pi) = -Q(\varphi_{\text{CEP}})$, which is a direct consequence of symmetry: adding π to the CEP is equivalent to substituting $\mathcal{E}(t)$ with $-\mathcal{E}(t)$, which is equivalent to replacing x with $-x$ in our symmetric arrangement. One also infers from Fig. 7 that the relaxation rate of interband coherences influences the positions of minima and maxima of $Q(\varphi_{\text{CEP}})$, which is not the case for the phonon scattering rate γ .

Increasing the amplitude of the input laser fields, we reach the regime where even electrons initially excited in the middle of the Brillouin zone experience reflections at its edges during the laser pulse—dynamical Bloch oscillations (DBOs) take place. This is illustrated in Fig. 8, where we plot the outcomes of a simulation with a laser pulse that has a peak amplitude of the electric field of 10 GV m^{-1} , the other parameters being the same as in

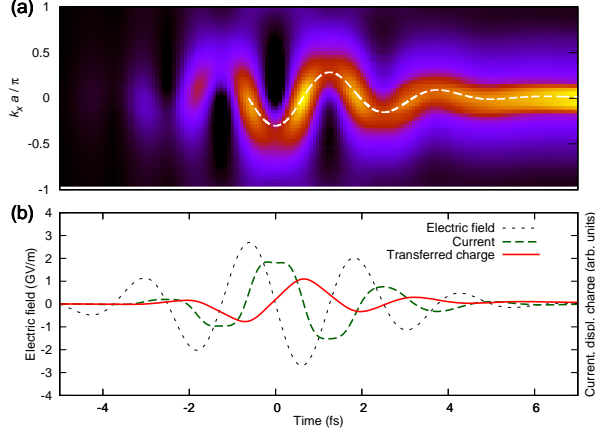


Figure 6: The same as Fig. 5, but for a sine pulse ($\varphi_{\text{CEP}} = \pi/2$). The semiclassical trajectory begins at the first main maximum of the laser field intensity, i.e. at $t = -\pi(2\omega_0)^{-1} \approx 0.6$ fs, and it trespasses $\mathbf{k} = 0$ at the peak of the next half-cycle, which is the starting point of the second dominant electron trajectory.

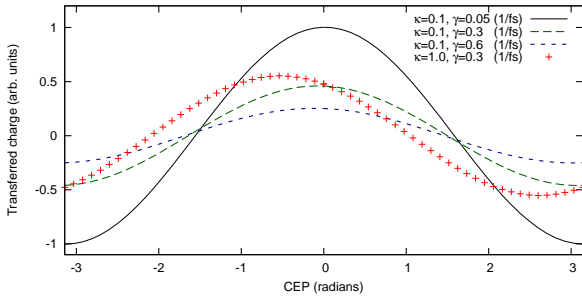


Figure 7: The dependence of the total charge transferred by a laser pulse on its carrier-envelope phase (CEP). The parameters are $\mathcal{E}_0 = 2 \text{ GV m}^{-1}$, $\tau = 2.3$ fs, $\gamma = 0.3 \text{ fs}^{-1}$. The curve corresponding to $\kappa = 0.1$, $\gamma = 0.05 \text{ fs}^{-1}$ has been normalized; the other ones have been scaled by the same number, i.e. the amplitudes of the curves relative to each other are kept fixed. Note that we use $\kappa = 0.1$, $\gamma = 0.3 \text{ fs}^{-1}$ in the following.

the previous simulations. DBOs occur in spite of the fact that we use a fairly large value for the electron-phonon scattering rate ($\gamma = 0.3 \text{ fs}^{-1}$). In contrast to the case of a low field (Fig. 5), the final transferred charge is now negative, which can be interpreted in terms of the semiclassical electron displacement. The dominant electron trajectory, shown as a dashed white line, crosses the lower edge of the Brillouin zone, but it doesn't reach its upper edge. Since $\mathbf{v}_c(\mathbf{k}) = 0$ at the edges of the Brillouin zone, the electron is displaced most during the time when $k_x > 0$. Consequently, the final electron displacement is positive, and the transferred charge is negative.

Note that the temporal evolution of the current in Fig. 8 contains frequency components higher than those of the driving field. The same effect in a different param-

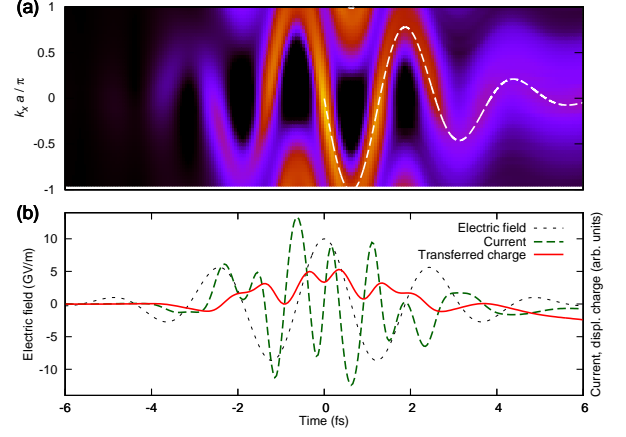


Figure 8: The effect of dynamical Bloch oscillations in a simulation with the following parameters: $\mathcal{E}_0 = 10 \text{ GV m}^{-1}$, $\varphi_{\text{CEP}} = 0$, $\tau = 2.3$ fs, $\kappa = 0.1 \text{ fs}^{-1}$, $\gamma = 0.3 \text{ fs}^{-1}$. (a) Time evolution of the conduction-band electron population $n_c(k_x, t)$ for a laser field with an amplitude sufficient for accelerating excited electrons to the edges of the Brillouin zone. The white dashed line represent the solution of Eq. (6) with $\mathbf{k}(0) = 0$. (b) The electric field of the laser pulse $\mathcal{E}_x(t)$, the induced current density j_x and the transferred charge $Q(t)$.

eter regime was reported to contribute to the generation of nonperturbative high-order harmonics in solids [14].

Figs. 5 and 8 demonstrate that DBOs have a big impact on the CEP dependence of the transferred charge $Q(\varphi_{\text{CEP}})$. In Fig. 9, we investigate it more systematically by plotting the normalized transferred charge

$$\tilde{Q}(\varphi_{\text{CEP}}, \mathcal{E}_0) = \frac{Q(\varphi_{\text{CEP}}, \mathcal{E}_0)}{\langle n_c \rangle_{\text{max}}(\mathcal{E}_0)} \quad (11)$$

for different laser intensities. The \mathcal{E}_0 dependent normalization factor

$$\langle n_c \rangle_{\text{max}}(\mathcal{E}_0) = \max_t \left(\frac{\int_{\text{BZ}} n_c(\mathbf{k}, \mathcal{E}_0, t, \varphi_{\text{CEP}} = 0) d^2\mathbf{k}}{\int_{\text{BZ}} d^2\mathbf{k}} \right), \quad (12)$$

which is plotted in Fig. 9(c), denotes the maximum of the time dependent average population in the conduction band for $\varphi_{\text{CEP}} = 0$.

One immediately observes that the extrema of $Q(\varphi_{\text{CEP}})$ shift as the laser intensity increases. By inspecting these simulations, we identified DBOs for peak laser fields above 7 GV m^{-1} . Below this limit, $Q(\varphi_{\text{CEP}})$ is approximately proportional to $\cos(\varphi_{\text{CEP}})$, and only the amplitude of $Q(\varphi_{\text{CEP}})$ increases with the peak laser intensity. For intensities high enough to induce DBOs, the extrema of $Q(\varphi_{\text{CEP}})$ change their positions. For $\mathcal{E}_0 = 15 \text{ GV m}^{-1}$, maxima and minima exchange their places.

To relate these observations to the semiclassical analysis, we focus on the cosine pulse and plot the electron displacement at $t_{\text{max}} = 15$ fs as a function of the peak

electric field in Fig. 9(a). We see that this analysis qualitatively explains our numerical results: $Q(\varphi_{\text{CEP}} = 0, \mathcal{E}_0)$ and $s(t_0 = 0, \mathcal{E}_0)$ have their extrema at approximately the same values of the peak electric field \mathcal{E}_0 .

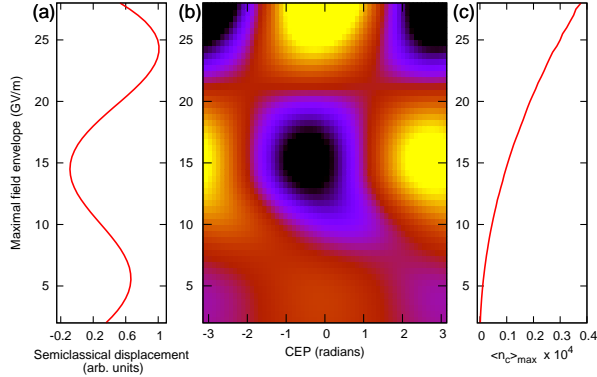


Figure 9: (a) The semiclassical electron displacement (10) for $\varphi_{\text{CEP}} = 0$, $t_0 = 0$ and $t_{\text{max}} = 15$ fs. The parameters of the laser pulse are $\tau = 2.3$ fs and $\omega_0 = 2.51$ fs $^{-1}$. (b) The normalized transferred charge \tilde{Q} , defined by Eq. (11), as a function of the CEP and the amplitude of the laser pulse. For dephasing and relaxation, we used $\kappa = 0.1$ fs $^{-1}$ and $\gamma = 0.3$ fs $^{-1}$. (c) The maximal average population in the conduction band $\langle n_c \rangle_{\text{max}}(\mathcal{E}_0)$, defined by Eq. (12), for $\varphi_{\text{CEP}} = 0$.

IV. SUMMARY

Using an admittedly simple model, we have investigated the multiphoton injection and laser-driven motion

of charge carriers in a wide gap bulk dielectric exposed to intense few-cycle laser pulses. Our most important finding is that whenever a laser field drives electrons close to or beyond the edges of the Brillouin zone, this has a significant impact on CEP sensitive measurements like those reported in [17]. This effect survives even if we account for dephasing and assume electron-phonon scattering rates as high as $\gamma \sim 10^{14}$ s $^{-1}$, which is close to scattering rates reported for SiO $_2$ [20, 21]. Thus, the detection of the total transferred charge can be used to measure signatures of dynamical Bloch oscillations in bulk solids. Furthermore, we show that this effect can be qualitatively explained by evaluating the semiclassical electron displacement for dominant electron trajectories.

Acknowledgements

The authors are indebted to A. Schiffrin, S. Kruchinin, F. Krausz and, particularly, N. Karpowicz for illuminating discussions. This work was supported by the Hungarian Scientific Research Fund (OTKA) under Contract No. T81364 as well as by the projects TÁMOP-4.2.2.A-11/1/KONYV-2012-0060 and TÁMOP-4.2.2.C-11/1/KONYV-2012-0010 supported by the European Union and co-financed by the European Social Fund. V.S.Y. acknowledges support by the DFG Cluster of Excellence: Munich-Centre for Advanced Photonics.

-
- [1] F. Bloch, *Zeitschrift für Physik* **52**, 555 (1929).
 - [2] G. H. Wannier, *Phys. Rev.* **117**, 432 (1960).
 - [3] W. V. Houston, *Phys. Rev.* **57**, 184 (1940).
 - [4] E. E. Mendez, F. Agulló-Rueda, and J. M. Hong, *Phys. Rev. Lett.* **60**, 2426 (1988).
 - [5] J. Feldmann, K. Leo, J. Shah, D. A. B. Miller, J. E. Cunningham, T. Meier, G. von Plessen, A. Schulze, P. Thomas, and S. Schmitt-Rink, *Phys. Rev. B* **46**, 7252 (1992).
 - [6] M. Ben Dahan, E. Peik, J. Reichel, Y. Castin, and C. Salomon, *Phys. Rev. Lett.* **76**, 4508 (1996).
 - [7] T. Pertsch, P. Dannberg, W. Elfle, A. Bräuer, and F. Lederer, *Phys. Rev. Lett.* **83**, 4752 (1999).
 - [8] R. Morandotti, U. Peschel, J. S. Aitchison, H. S. Eisenberg, and Y. Silberberg, *Phys. Rev. Lett.* **83**, 4756 (1999).
 - [9] R. Sapienza, P. Costantino, D. Wiersma, M. Ghulinyan, C. J. Oton, and L. Pavesi, *Phys. Rev. Lett.* **91**, 263902 (2003).
 - [10] V. Agarwal, J. A. del Rio, G. Malpuech, M. Zamfirescu, A. Kavokin, D. Coquillat, D. Scalbert, M. Vladimirova, and B. Gil, *Phys. Rev. Lett.* **92**, 097401 (2004).
 - [11] M. Holthaus, *Journal of Optics B: Quantum and Semi-classical Optics* **2**, 589 (2000).
 - [12] J. A. Gruetzmacher and N. F. Scherer, *Review of Scientific Instruments* **73**, 2227 (2002).
 - [13] E. Goulielmakis, M. Schultze, M. Hofstetter, V. S. Yakovlev, and J. Gagnon, *Science* **320**, 1614 (2008), ISSN 0036-8075.
 - [14] S. Ghimire, A. D. DiChiara, E. Sistrunk, P. Agostini, L. F. DiMauro, and D. A. Reis, *Nat. Physics* **7**, 138 (2011).
 - [15] S. Ghimire, A. D. DiChiara, E. Sistrunk, U. B. Szafruga, P. Agostini, L. F. DiMauro, and D. A. Reis, *Phys. Rev. Lett.* **107**, 167407 (2011).
 - [16] D. Golde, T. Meier, and S. W. Koch, *Phys. Rev. B* **77**, 201407 (2008).

- 075330 (2008).
- [17] A. Schiffrin, T. Paasch-Colberg, N. Karpowicz, V. Apalkov, D. Gerster, S. Muhlbrandt, M. Korbman, J. Reichert, M. Schultze, S. Holzner, et al., *Nature advance online publication* (2012), ISSN 1476-4687, URL <http://dx.doi.org/10.1038/nature11567>.
 - [18] A. Baltuska, T. Udem, M. Uiberacker, M. Hentschel, and E. Goulielmakis, *Nature* **421**, 611 (2003).
 - [19] V. Apalkov and M. I. Stockman, *Phys. Rev. B* **86**, 165118 (2012).
 - [20] R. C. Hughes, *Phys. Rev. Lett.* **30**, 1333 (1973).
 - [21] M. V. Fischetti, D. J. DiMaria, S. D. Brorson, T. N. Theis, and J. R. Kirtley, *Phys. Rev. B* **31**, 8124 (1985).
 - [22] F. Quéré, S. Guizard, P. Martin, G. Petite, H. Merdji, B. Carré, J.-F. Hergott, and L. Le Déroff, *Phys. Rev. B* **61**, 9883 (2000).
 - [23] L. W. Casperson, *Phys. Rev. A* **57**, 609 (1998).
 - [24] H. Haug and S. W. Koch, *Quantum Theory of the Optical and Electronic Properties of Semi conductors* (World Scientific, New Jersey, London, Singapore, 2004), 4th ed.
 - [25] M. Wegener, *Extreme Nonlinear Optics: An Introduction*, Advanced Texts in Physics (Springer, 2004), ISBN 9783540222910.
 - [26] T. Otobe, M. Yamagiwa, J.-I. Iwata, K. Yabana, T. Nakatsukasa, and G. F. Bertsch, *Phys. Rev. B* **77**, 165104 (2008).
 - [27] O. D. Mücke, *Phys. Rev. B* **84**, 081202 (2011).
 - [28] C. Kittel, *Introduction to solid state physics* (Wiley, New York, 2005), 8th ed.
 - [29] E. Yablonovitch, J. P. Heritage, D. E. Aspnes, and Y. Yafet, *Phys. Rev. Lett.* **63**, 976 (1989).